

Proton impact on ground and excited states of atomic hydrogen

Anthony C. K. Leung* and Tom Kirchner†

Department of Physics and Astronomy, York University, Toronto, Ontario, M3J 1P3, Canada

(Dated: December 10, 2019)

The processes of electron excitation, capture, and ionization were investigated in proton collisions with atomic hydrogen in the initial $n = 1$ and $n = 2$ states at impact energies from 1 to 300 keV. The theoretical analysis is based on the close-coupling two-center basis generator method in the semiclassical approximation. Calculated cross sections are compared with previous results which include data obtained from classical-trajectory Monte Carlo, convergent close-coupling, and other two-center atomic orbital expansion approaches. There is an overall good agreement in the capture and excitation cross sections while there are some discrepancies in the ionization results at certain impact energies. These discrepancies in the present results can be partially understood through the use of a $1/n^3$ scaling model.

arXiv:1907.08234v2 [physics.atom-ph] 7 Dec 2019

* leungant@yorku.ca

† tomk@yorku.ca

I. INTRODUCTION

The classic problem of proton scattering from ground-state hydrogen has often been used as a benchmark system for theoretical models [1–5]. Cross sections of electronic processes (e.g., capture, excitation, and ionization) for this prototypical system have important applications in plasma physics. In recent times, there is much interest from the International Thermonuclear Experimental Reactor (ITER) fusion energy research community [6] in ion collisions with initially excited hydrogen atoms. The International Atomic Energy Agency (IAEA) Coordinated Research Program on Data for Atomic Processes of Neutral Beams in Fusion Plasma aims to provide recommended data to the ITER project for plasma modeling [7].

Theoretical efforts using classical and semiclassical approaches have been made to obtain cross sections for proton collisions with excited hydrogen atoms. Previously, Pindzola et al. [8] performed calculations for capture and excitation cross sections for p -H($2s$) collisions at impact energies from 1 to 100 keV by using the classical-trajectory Monte Carlo (CTMC), the two-center atomic-orbital close-coupling with pseudostates (AOCC-PS), and the time-dependent lattice (TDL) approaches. Recent work based on the wave packet convergent close-coupling (WP-CCC) method [9] and a two-center atomic-orbital close-coupling with Gaussian-type orbitals (AOCC-GTO) calculation [10] reported similar analyses and also examined p -H($2p_0$) and p -H($2p_1$) collisions. Comparisons of the capture cross sections of p -H($2s$) collisions from these calculations all showed good agreement but there are discrepancies in the excitation results from 10 to 100 keV impact energy. These discrepancies could be due to differences in the target basis size which has been larger in the recent works [9, 10] than in the AOCC-PS analysis [8]. These differences could indicate that these additional states serve as intermediate channels during the collision. Ionization cross sections from the WP-CCC calculations were also reported but no comparisons were made since no other data were available at the time.

The purpose of the present work is to address the need for additional independent analyses of proton collisions with hydrogen atoms for the IAEA Coordinated Research Program to help establish the range of validity of cross section data. The approach for the present theoretical analysis is the semiclassical, nonperturbative two-center basis generator method (TC-BGM) [11]. It is a close-coupling approach similar to the AOCC method, but the main feature of the TC-BGM is its use of a dynamic basis that is adapted to the problem at hand. This has the practical advantage that fewer pseudostates need to be employed to reach convergence compared to using the standard approach. In this work, the focus is on proton collisions with atomic hydrogen in the initial $n = 1$ and $n = 2$ states at impact energies from 1 to 300 keV. This is the region where the discrepancies of excitation and ionization cross sections are largest based on previous comparisons [9]. It is the aim of this study to provide some validation of the existing results.

The article is organized as follows. In Sect. II the TC-BGM is outlined. The collision cross section results are presented and discussed in Sect. III. Finally, concluding remarks are provided in Sect. IV. Atomic units ($\hbar = e = m_e = 4\pi\epsilon_0 = 1$) are used throughout the article unless stated otherwise.

II. TWO-CENTER BASIS GENERATOR METHOD

The present treatment of the proton-hydrogen collision problem starts with the impact-parameter model within the semiclassical approximation. Figure 1 shows the setup of the collision framework where the xz -plane is chosen as the scattering plane. In the laboratory frame, the hydrogen atom is assumed to be fixed in space and the proton travels in a straight-line path at constant speed v_p , described by $\mathbf{R}(t) = (b, 0, v_p t)$, where b is the impact parameter.

In a one-electron collision system, the objective is to solve a set of single-particle time-dependent Schrödinger equations (TDSEs) for the initially occupied ground and excited states under consideration,

$$i \frac{\partial}{\partial t} \psi_j(\mathbf{r}, t) = \hat{h}(t) \psi_j(\mathbf{r}, t), \quad j = 1, \dots, K. \quad (1)$$

For the proton-hydrogen collision system, the target is described by the undisturbed Hamiltonian \hat{h}_0 which contains the electronic kinetic energy and the Coulomb potential of the target nucleus. Let $\hat{V}(t)$ be the time-dependent Coulomb potential of the proton projectile. The Hamiltonian of the collision system is

$$\begin{aligned} \hat{h}(t) &= \hat{h}_0 + \hat{V}(t) \\ &= -\frac{1}{2} \nabla^2 - \frac{1}{r} - \frac{1}{|\mathbf{r} - \mathbf{R}(t)|}. \end{aligned} \quad (2)$$

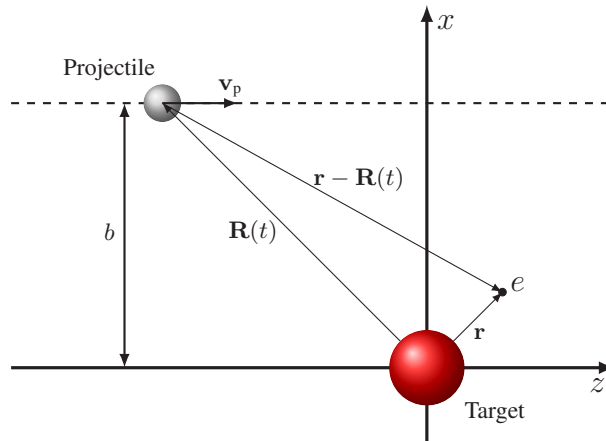


FIG. 1. Setup of the collision system in the impact parameter model.

The present calculation solves the set of single-particle TDSEs (1) by the close-coupling approach subject to all bound states of the hydrogen target in the $n = 1$ and $n = 2$ shells as initially occupied states.

The idea of the close-coupling TC-BGM is to expand the electronic solutions $\psi_j(\mathbf{r}, t)$ in a basis which dynamically adapts to the time-dependent problem. In an early foundational work of the single-center BGM [12], it was argued that the model space constructed by repeated application of a regularized Coulombic projectile potential onto atomic target eigenstates provides such a dynamical representation of $\psi_j(\mathbf{r}, t)$. Calculations in a two-center framework are naturally performed in the center-of-mass frame. The basis is then generated from a finite set of N_T target and $N - N_T$ projectile atomic states taking into account Galilean invariance by the appropriate choice of electron translation factors

$$\phi_\nu^0(\mathbf{r}) = \begin{cases} \phi_\nu(\mathbf{r}_T) \exp(i\mathbf{v}_T \cdot \mathbf{r}), & \nu \leq N_T \\ \phi_\nu(\mathbf{r}_P) \exp(i\mathbf{v}_P \cdot \mathbf{r}), & \text{otherwise,} \end{cases} \quad (3)$$

where \mathbf{v}_T and \mathbf{v}_P are the velocities of the target and projectile frames with respect to the center-of-mass frame, respectively. In the TC-BGM, the generating two-center atomic basis (3) is augmented by BGM pseudostates, which are constructed by repeated application of a regularized potential onto the target states only,

$$\chi_\nu^\mu(\mathbf{r}, t) = [W_P(t)]^\mu \phi_\nu^0(\mathbf{r}), \quad \mu = 1, \dots, M, \quad (4)$$

$$W_P(t) = \frac{1 - \exp[-\alpha r_P(t)]}{r_P(t)}, \quad (5)$$

where $\alpha = 1$ is used in practice. The construction of Eq. (4) is what gives the basis of ψ_j a dynamical feature. The set of pseudostates (4), when orthogonalized to the generating basis (3), accounts for quasimolecular effects at low impact energies and for ionization channels.

In terms of the basis states χ_ν^μ , the single-particle solution for the j -th initial condition is represented as

$$\psi_j(\mathbf{r}, t) = \sum_{\mu=0}^{M(\nu)} \sum_{\nu=1}^N c_{\mu\nu}^j(t) \chi_\nu^\mu(\mathbf{r}, t), \quad (6)$$

$$M(\nu) = \begin{cases} M & \text{if } \nu \leq N_T \\ 0 & \text{otherwise.} \end{cases}$$

Substituting Eq. (6) into Eq. (1) and projecting onto the BGM basis states results in a set of close-coupling differential equations which can be expressed in matrix-vector form

$$iS \frac{d}{dt} \mathbf{c} = \mathbf{M} \mathbf{c}, \quad (7)$$

where \mathbf{c} is a column vector with the expansion coefficients as components, \mathbf{S} is the overlap matrix and \mathbf{M} is the interaction matrix. Equation (7) can be solved by standard methods. Probabilities of electronic transitions at given impact parameter and speed are obtained from the expansion coefficients in the asymptotic region

$$p_{\mu\nu}^j = \lim_{t \rightarrow \infty} |c_{\mu\nu}^j(t)|^2. \quad (8)$$

Specifically, bound-state probabilities for finding the electron on the target p^{tar} or on the projectile p^{cap} are calculated from summing up the transition probabilities within the generating basis (3), and probabilities for total ionization p^{ion} are obtained from the unitarity criterion

$$p^{\text{ion}} = 1 - p^{\text{tar}} - p^{\text{cap}}. \quad (9)$$

Cross sections for the electronic transitions are obtained by integrating the probabilities over the impact parameter

$$\sigma = 2\pi \int_0^{b_{\text{max}}} bp(b)db, \quad (10)$$

where b_{max} is the upper bound at which the integral is cut in practice. It should be noted that the conservation of unitarity (9) was monitored in the present analysis and it was found that deviations produced by the calculations are typically no larger than 1%.

In the present analysis, the basis set $\{\chi_\nu^\mu\}$ includes all nlm hydrogen states for $n \in [0, 6]$ on both the target and projectile. The basis also includes a set of BGM pseudostates up to order $\mu = 3$. Table I shows an example of results from a convergence test for the p -H($2s$) system at $E_P = 15$ keV where the number of BGM pseudostates was systematically increased until the percent differences of cross section results are about 1% or less. Furthermore, four initial states of the hydrogen target $\{1s, 2s, 2p_0, 2p_1\}$ are considered in the present calculation. It is noteworthy that probabilities from collision calculations for the $2p_1$ and $2p_{-1}$ initial state are identical due to the symmetry of the collision system. Propagation of the set of TDSEs was carried out from $z_i = v_P t_i = -100$ to $z_f = v_P t_f = 100$ a.u. for each impact parameter from $b_{\text{min}} = 0.3$ to $b_{\text{max}} = 70$ a.u. Note that the integration of Eq. (10) is still performed over the interval $[0, b_{\text{max}}]$. Preliminary calculations showed that excitation from initially excited states to final target states of higher angular momentum decays slowly with increasing impact parameter. Therefore, the choice of $b_{\text{max}} = 70$ a.u. in the present calculation was necessary to capture the asymptotic profile of these transition probabilities with sufficient accuracy.

TABLE I. Total cross sections (10^{-16} cm²) for p -H($2s$) collisions at $E_P = 15$ keV with different number of BGM pseudostates.

Total pseudostates	σ^{cap}	σ^{ion}
126	6.96	18.62
175	6.62	20.72
192	6.57	21.02
203	6.58	21.24

III. RESULTS AND DISCUSSION

To alleviate the discussion of the results, only the main findings and comparisons are highlighted in this section. Detailed results from this analysis such as state-selective capture are available from the authors upon request.

Results of the nl excitation cross sections for p -H($1s$) and p -H($2s$) collisions are displayed in Fig. 2. For H($1s$) collisions, the present cross sections are compared with several previous theoretical results based on the TDL technique [2, 8], close-coupling approaches based on a large Sturmian basis (Sturmian-CC) [4], semiclassical convergent close-coupling (SC-CCC) calculations [5], and the AOCC-GTO analysis [10]. Note that the uncertainty bars shown from the AOCC-GTO results are estimates of the convergence of the cross sections [10]. Previous experimental results of Refs. [13, 14] are shown alongside. For H($2s$) collisions, the present cross sections are shown together with the aforementioned works based on the AOCC-PS [8], CTMC [8], WP-CCC [9] and AOCC-GTO [10] calculations. Although many earlier works on p -H($1s$) collisions exist in the literature

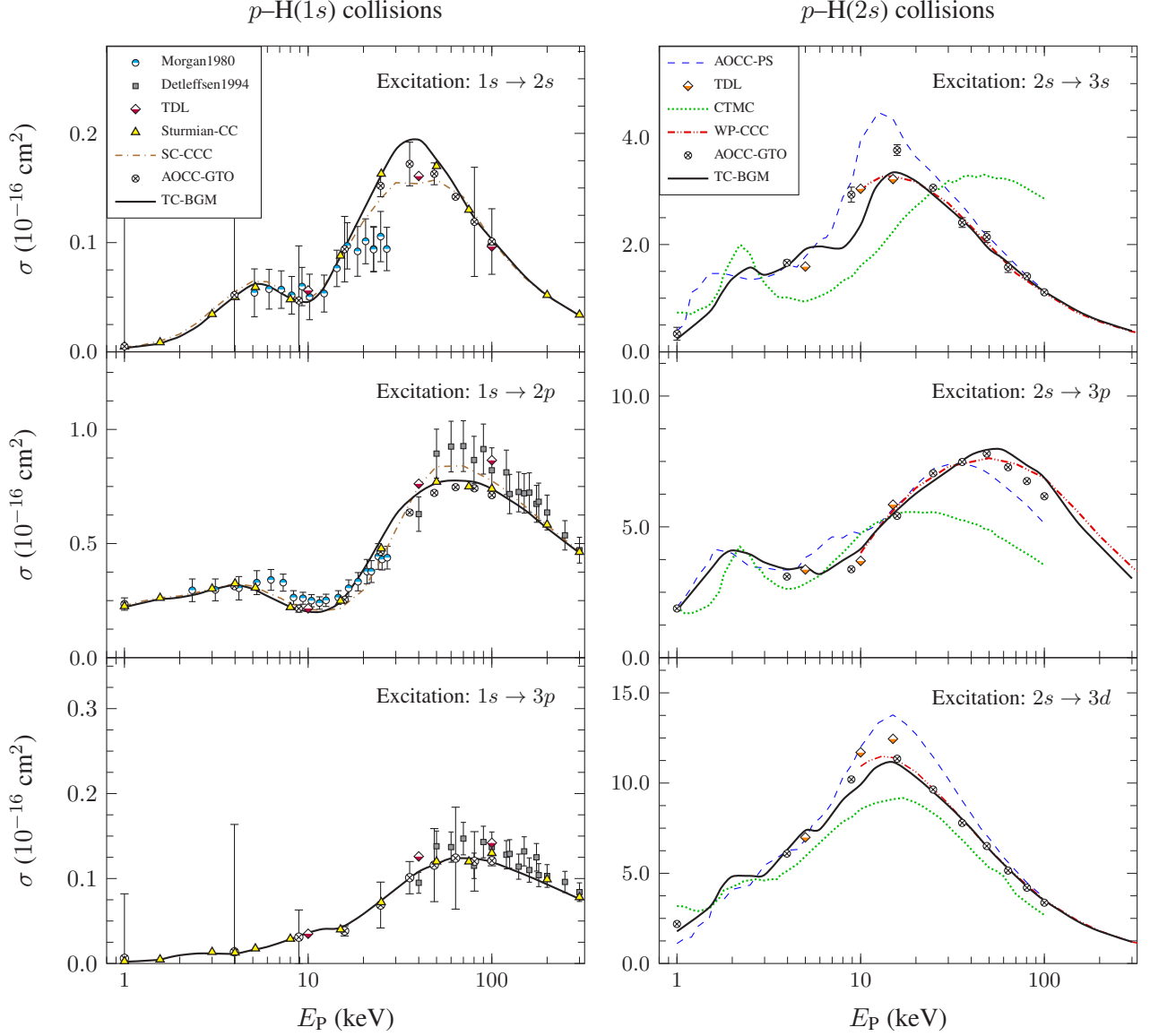


FIG. 2. State-selective excitation cross sections plotted with respect to the impact energy for p -H($1s$) (left column) and p -H($2s$) collisions (right column). Experiment: Morgan1987 [13] and Detleffsen1994 [14]. Theory: AOCC-PS, CTMC and TDL [8]; Sturmiian-CC [4]; SC-CCC [5]; WP-CCC [9]; AOCC-GTO [10]; and present TC-BGM.

such as the AOCC calculations of Refs. [15, 16], the present comparison focuses on theoretical works within the past decade.

Examining the present excitation results for H($1s$) collisions, the cross section profile for all three transitions exhibits a similar feature where the cross section peaks at an impact energy between 10 and 100 keV. Quantitatively, the $1s \rightarrow 2p$ transition is largest compared to the other two transitions. Furthermore, the present TC-BGM results are in excellent agreement with the Sturmiian-CC results [4] for all three transitions. Similar agreement can also be seen with other calculations except around 40 keV where discrepancies are more pronounced. Although there are also some quantitative discrepancies with the experimental data [13, 14], for example between 50 and 100 keV for the $1s \rightarrow 2p$ transition, the present results are mostly within the uncertainty range.

Similar observations can be made for the excitation cross sections for H($2s$) collisions. Specifically, these cross sections also peak in the energy region between 10 and 100 keV. However, the excitation cross sections for H($2s$) collisions are larger in magnitude than those of H($1s$) collisions. From the comparisons with previous

results, it can be seen that the present TC-BGM calculations from 1 to 10 keV are mostly consistent with the AOCC-GTO [10], AOCC-PS and TDL results [8] and follow the WP-CCC [9] trends at higher energies while the discrepancies with AOCC-PS are more pronounced in this regime. Although the cross section curves from the CTMC calculations [8] have similar structures as the other results, quantitative differences in the intermediate region are apparent. Moreover, although both the present TC-BGM and the AOCC approaches utilize a basis-set expansion technique in the semiclassical approximation, the discrepancies between the TC-BGM and both AOCC data sets [8, 10] may be attributed to the differences in the basis. Both AOCC-PS [8] and AOCC-GTO [10] calculations included bound states of hydrogen with angular momenta up to $l = 4$ compared to $l = 5$ in the present calculations. However, the AOCC-GTO calculation has more pseudostates included in the basis than the AOCC-PS calculation, which may explain the discrepancies between those results. Additional TC-BGM calculations also showed that a reduced basis on the target, for example including all nlm states up to $n = 5$ only, had larger discrepancies with the WP-CCC results at 15 keV. However, such a change of the basis does not necessarily affect the excitation cross sections at all impact energies.

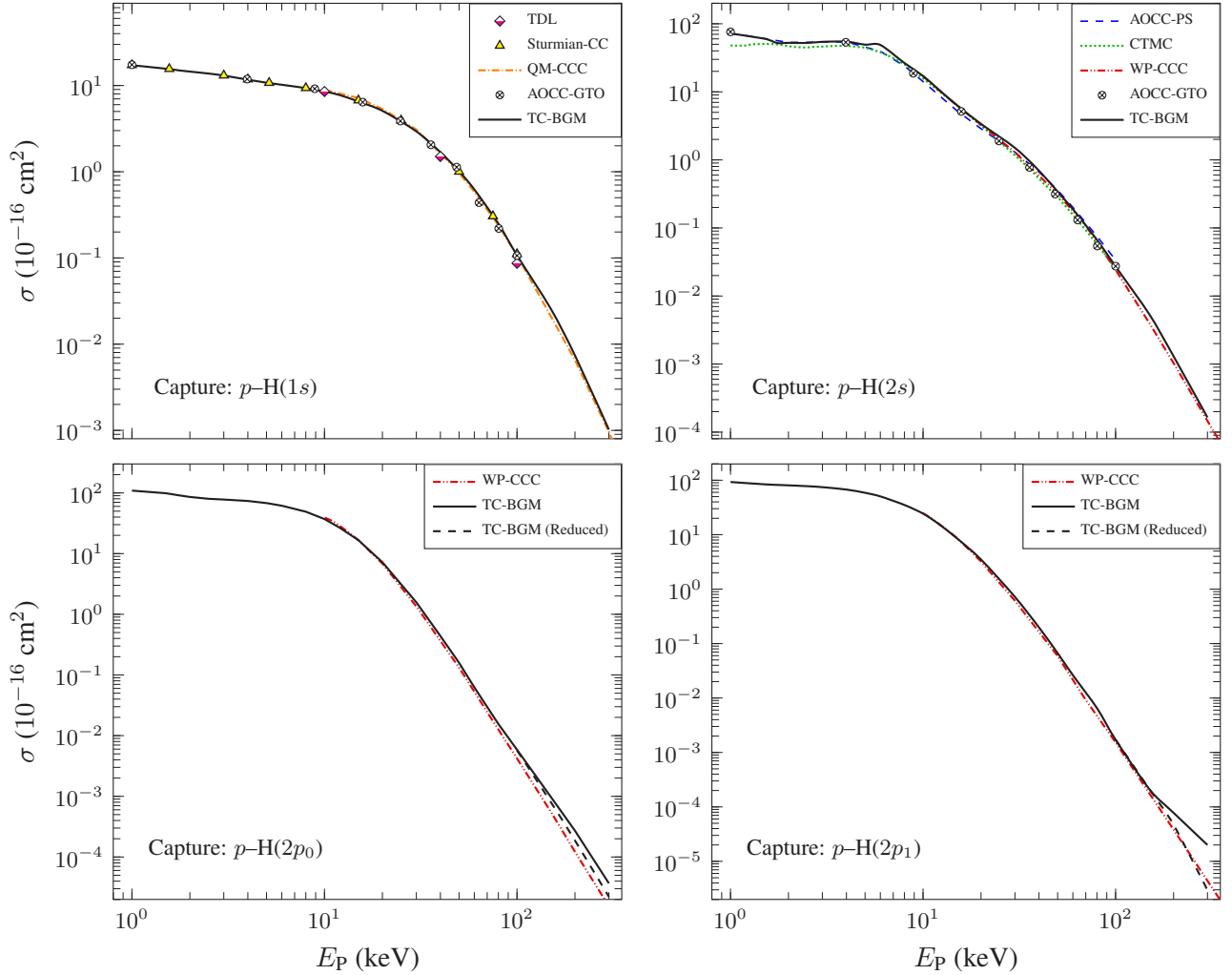


FIG. 3. Total capture cross sections for the proton–hydrogen collision problem. Calculations include: TDL [2]; AOCC-PS and CTMC [8]; Sturmian-CC [4]; QM-CCC [17]; WP-CCC [9]; AOCC-GTO [10]; and present TC-BGM.

Figure 3 shows the total capture cross sections plotted with respect to the impact energy for the p -H scattering system. Calculations for the four initial states of the hydrogen target $\{1s, 2s, 2p_0, 2p_1\}$ are shown in separate plots. Theoretical results from the aforementioned studies [2, 4, 8, 9] are shown alongside the present results. For H($1s$) collisions the included results from Ref. [17] are from calculations based on the quantum-mechanical convergent close-coupling (QM-CCC) method, which is viewed as an exact treatment of the quantum-mechanical three-body Schrödinger equation. It is noteworthy that the AOCC-GTO calculation [10] considered all $2p_m$

initial states, but the reported cross sections are averaged over the m substates, and thus, not appropriate to compare with the results shown in the present figure. Comparisons of the present TC-BGM capture cross sections for H($2p$) collisions, when averaged across the m states, agree with the AOCC-GTO calculation within 2% or better.

The present capture results show the expected fall-off with increasing energy. At low energies from 1 to 10 keV, the cross sections for H($n = 2$) collisions are larger than those of H($n = 1$) collisions. In general, the present results are in very good agreement with previous calculations [2, 4, 9, 17]. Although there is good qualitative agreement between the present results and the WP-CCC calculations for the p -H($2p_0$) and p -H($2p_1$) systems, quantitative discrepancies are apparent at 100 keV and higher. Further investigation showed that the TC-BGM capture into the $n = 6$ shell is about an order of magnitude larger than the capture into lower shells at these energies, which appears to indicate a numerical precision issue. This is evident when capture channels from higher n -states that do not follow the expected distribution are excluded from the sum as shown in Fig. 3 as “TC-BGM (Reduced)”, resulting in a total cross section that is closer to the WP-CCC result. While in principle these cross section can be improved by fine-tuning numerical parameters in the calculations this is rather cumbersome for this problem since, for example, slightly reducing the grid points leads to convergence problems while a slightly denser grid creates a significant increase in computation time. In view of these difficulties, no adjustments were made to improve the numerical accuracy of the calculations at high energies.

In Fig. 4, several sets of ionization cross sections for H($n = 1$) and H($n = 2$) collisions are compared with the present TC-BGM results. The sets include experimental measurements by Shah and co-workers [18–20] along with theoretical data from QM-CCC [17], WP-CCC [9], and AOCC-GTO [10] approaches. Additional results based on a scaling model are also presented for comparison in order to help understand some of the discrepancies shown in the present results. The use of this scaling model is explained as follows.

The well-known $1/n^3$ scaling law from perturbation theory [21] was applied to the present results to extrapolate transitions to higher n -shells. For capture, if p_n is the probability of transfer into the n -th shell of the projectile an assumed $1/n^3$ scaling predicts that

$$p_{n+k} = \left(\frac{n}{n+k} \right)^3 p_n, \quad k = 1, 2, \dots \quad (11)$$

is the probability of transfer into the $(n+k)$ -shell of the projectile. A detailed analysis showed that using the present results for capture into $n = 3, 4,$ or 5 to predict the capture into higher shells approximately fulfilled this scaling model. Although Eq. (11) applies to electron capture [21] the present analysis suggests that the excitation results also approximately follow this scaling law. The exception to Eq. (11) is capture from H($1s$) at low energies since the process is highly selective to a particular n -shell and the drop-off in higher shells does not follow the $1/n^3$ scaling. Moreover, the analysis showed that using the O -shell as the reference point where $n = 5$ is fixed in Eq. (11) yielded probabilities for higher n -shells that are modest in magnitude (i.e., neither too small nor too large) compared to using other reference shells. This scaling model in the present analysis is referred to as the O -shell model. With probabilities of the electronic transitions to higher n -shells computed in this way, new ionization probabilities are obtained from the unitarity criterion (9). By denoting $n' = n + k$, several choices of n' were made to obtain additional sets of ionization cross sections. As shown in Fig. 4, states up to $n' = 7$ were mainly considered in the low-energy region while states up to $n' = 10$ were considered in the intermediate region. The extreme case of $n' \rightarrow \infty$, which in practice is computed up to $k = 200$, is also included for comparison. Note that the scaling results for the latter two cases are not shown in the low-energy region since large sums of Eq. (11) turned out to violate the unitarity criterion (9) at those energies.

It is expected that ionization is significant in the intermediate energy regime between 10 keV and 1 MeV. Starting with ionization from p -H($1s$) collisions, the present TC-BGM cross sections reflect this behavior. In terms of comparisons, the present TC-BGM results are in good agreement with the Sturmian-CC results [4]. Although the present cross sections are consistent with the QM-CCC and AOCC-GTO results at and below 50 keV, there are some noticeable quantitative differences at higher energies. Based on the use of the scaling model (11), transitions to $n > 6$ states are insignificant, which suggests that these discrepancies are likely due to numerical issues mentioned earlier rather than an issue with basis size.

For H($n = 2$) collisions, the ionization cross sections also show a maximum in the intermediate energy region. One should note that the cross sections for these collisions are larger in magnitude than those of H($n = 1$) collisions. It is evident from the comparisons between the present TC-BGM and the WP-CCC [9] results that there are some discrepancies in the vicinity of the maximum. The results of the scaling model (11) in the low-energy region show that additional states up to $n \approx 7$ are needed to approximately match the profile of the WP-CCC results. Note that the WP-CCC [9] considered angular momentum quantum numbers $l \in [0, 6]$ and had them assigned to $(10 - l)$ bound eigenstates on each center. For example, in the simplest case of $l = 0$

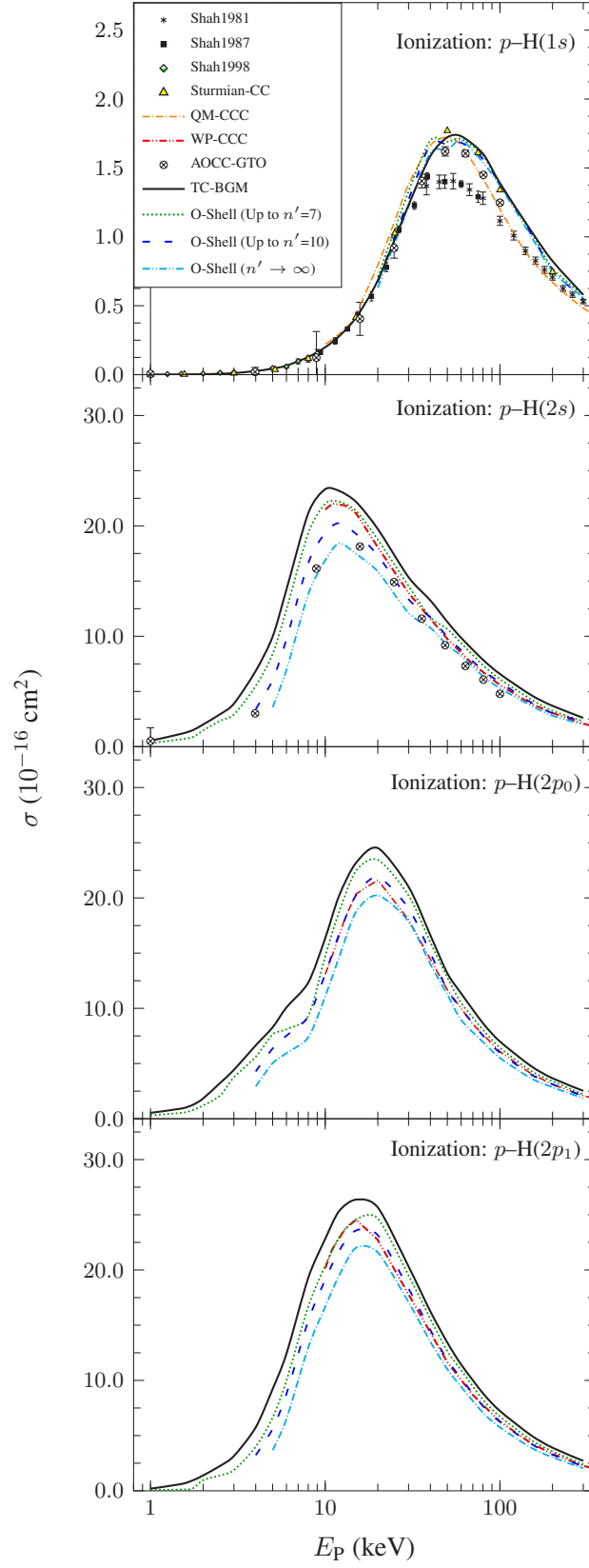


FIG. 4. Ionization cross sections plotted with respect to the impact energy for p -H collisions. Experiment: Shah1981 [18]; Shah1987 [19]; and Shah1998 [20]. Theory: QM-CCC [17]; WP-CCC [9]; AOCC-GTO [10]; and present TC-BGM.

there are 10 bound states on one center in the WP-CCC basis, which is more than the present basis of 6 bound states for the corresponding l quantum number. Therefore, the scaling model seems to suggest that additional bound states (either on the target, projectile, or both) may be required in the TC-BGM calculation to reach the same level of agreement with the WP-CCC results for $H(n=2)$ collisions as for $H(n=1)$ collisions. Moreover, results of the scaling model that involve much higher shells reduce the ionization cross sections further. Overall, considering that the quantitative differences between the TC-BGM and WP-CCC results are no more than approximately 15%, the results obtained from the TC-BGM calculations are deemed satisfactory.

IV. CONCLUDING REMARKS

The processes of electron excitation, capture, and ionization in proton collisions with atomic hydrogen were investigated for the $1s$, $2s$, $2p_0$, and $2p_1$ initial states. The present study focuses on collisions at impact energies from 1 to 300 keV. These processes were quantified by solving a set of single-particle TDSEs for the expansion coefficients by using the TC-BGM in the semiclassical approximation. Based on the close-coupling approach, the main feature of the TC-BGM is its construction of dynamically adapted states which allow for fewer pseudostates in the basis to reach convergence compared to the standard two-center AOCC with pseudostates approach.

Overall, the cross sections produced from the present TC-BGM calculation are in good agreement with previous results. In particular, the present cross sections are mostly similar to the results based on modern close-coupling implementations such as the the Sturmian-CC [4], the recent WP-CCC calculations [9], and the AOCC-GTO calculations [10]. The discrepancies between the present and previous calculations for ionization can be partially attributed to an insufficient number of bound states in the present analysis as shown by the use of a $1/n^3$ scaling model on the cross sections. Notwithstanding these issues, the capture and excitation results produced in this work can be viewed as a notable achievement of the TC-BGM in that a similar level of accuracy as in other close-coupling approaches is obtained with a smaller, dynamically-adapted basis.

V. ACKNOWLEDGMENTS

This work was funded by the Natural Sciences and Engineering Research Council of Canada (NSERC) and was made possible with the high-performance computing resources provided by Compute/Calcul Canada. We thank Alain Dubois and Nicolas Sisourat for discussions.

VI. AUTHORS CONTRIBUTION STATEMENT

A.C.K. Leung and T. Kirchner conceived the study, analyzed the results and drafted the manuscript. A.C.K. Leung performed the numerical calculations. Both the authors have read and approved the final manuscript.

-
- [1] R. Olson and A. Salop, *Phys. Rev. A* **16**, 531 (1977).
 - [2] A. Kolakowska, M. S. Pindzola, F. Robicheaux, D. R. Schultz, and J. C. Wells, *Phys. Rev. A* **58**, 2872 (1998).
 - [3] N. Toshima, *Phys. Rev. A* **59**, 1981 (1999).
 - [4] T. G. Winter, *Phys. Rev. A* **80**, 032701 (2009).
 - [5] S. K. Avazbaev, A. S. Kadyrov, I. B. Abdurakhmanov, D. V. Fursa, and I. Bray, *Phys. Rev. A* **93**, 022710 (2016).
 - [6] R. Hemsforth, H. Decamps, J. Graceffa, B. Schunke, M. Tanaka, M. Dremel, A. Tanga, H. De Esch, F. Geli, J. Milnes, T. Inoue, D. Marcuzzi, P. Sonato, and P. Zaccaria, *Nucl. Fusion* **49**, 045006 (2009).
 - [7] H. K. Chung, *Data for Atomic Processes of Neutral Beams in Fusion Plasma Summary Report of the First Research Coordination Meeting*, Tech. Rep. (International Atomic Energy Agency (IAEA), 2017).
 - [8] M. S. Pindzola, T. G. Lee, T. Minami, and D. R. Schultz, *Phys. Rev. A* **72**, 062703 (2005).
 - [9] I. B. Abdurakhmanov, S. U. Alladustov, J. J. Bailey, A. S. Kadyrov, and I. Bray, *Plasma Phys. Control. Fusion* **60**, 095009 (2018).
 - [10] H. Agheny, J. P. Hansen, A. Dubois, A. Makhoute, A. Taoutioui, and N. Sisourat, *At. Data Nucl. Data Tables* (2019).
 - [11] M. Zapukhlyak, T. Kirchner, H. J. Lüdde, S. Knoop, R. Morgenstern, and R. Hoekstra, *J. Phys. B* **38**, 2353 (2005).
 - [12] O. J. Kroneisen, H. J. Lüdde, T. Kirchner, and R. M. Dreizler, *J. Phys. A* **32**, 2141 (1999).
 - [13] T. J. Morgan, J. Stone, and R. Mayo, *Phys. Rev. A* **22**, 1460 (1980).

- [14] D. Detleffsen, M. Anton, A. Werner, and K. H. Schartner, *J. Phys. B* **27**, 4195 (1994).
- [15] J. Kuang and C. D. Lin, *J. Phys. B* **29**, 1207 (1996).
- [16] J. Kuang and C. D. Lin, *J. Phys. B* **29**, 5443 (1996).
- [17] I. B. Abdurakhmanov, A. S. Kadyrov, S. K. Avazbaev, and I. Bray, *J. Phys. B* **49**, 115203 (2016).
- [18] M. B. Shah and H. B. Gilbody, *J. Phys. B* **14**, 2361 (1981).
- [19] M. B. Shah, D. S. Elliott, and H. B. Gilbody, *J. Phys. B* **20**, 2481 (1987).
- [20] M. B. Shah, J. Geddes, B. M. McLaughlin, and H. B. Gilbody, *J. Phys. B* **31**, L757 (1998).
- [21] K. Omidvar, *Phys. Rev.* **153**, 121 (1967).

- [1] R. Olson and A. Salop, *Phys. Rev. A* **16**, 531 (1977).
- [2] A. Kolakowska, M. S. Pindzola, F. Robicheaux, D. R. Schultz, and J. C. Wells, *Phys. Rev. A* **58**, 2872 (1998).
- [3] N. Toshima, *Phys. Rev. A* **59**, 1981 (1999).
- [4] T. G. Winter, *Phys. Rev. A* **80**, 032701 (2009).
- [5] S. K. Avazbaev, A. S. Kadyrov, I. B. Abdurakhmanov, D. V. Fursa, and I. Bray, *Phys. Rev. A* **93**, 022710 (2016).
- [6] R. Hemsworth, H. Decamps, J. Graceffa, B. Schunke, M. Tanaka, M. Dremel, A. Tanga, H. De Esch, F. Geli, J. Milnes, T. Inoue, D. Marcuzzi, P. Sonato, and P. Zaccaria, *Nucl. Fusion* **49**, 045006 (2009).
- [7] H. K. Chung, *Data for Atomic Processes of Neutral Beams in Fusion Plasma Summary Report of the First Research Coordination Meeting*, Tech. Rep. (International Atomic Energy Agency (IAEA), 2017).
- [8] M. S. Pindzola, T. G. Lee, T. Minami, and D. R. Schultz, *Phys. Rev. A* **72**, 062703 (2005).
- [9] I. B. Abdurakhmanov, S. U. Alladustov, J. J. Bailey, A. S. Kadyrov, and I. Bray, *Plasma Phys. Control. Fusion* **60**, 095009 (2018).
- [10] H. Agueny, J. P. Hansen, A. Dubois, A. Makhoute, A. Taoutioui, and N. Sisourat, *At. Data Nucl. Data Tables* (2019).
- [11] M. Zapukhlyak, T. Kirchner, H. J. Lüdde, S. Knoop, R. Morgenstern, and R. Hoekstra, *J. Phys. B* **38**, 2353 (2005).
- [12] O. J. Kroneisen, H. J. Lüdde, T. Kirchner, and R. M. Dreizler, *J. Phys. A* **32**, 2141 (1999).
- [13] T. J. Morgan, J. Stone, and R. Mayo, *Phys. Rev. A* **22**, 1460 (1980).
- [14] D. Detleffsen, M. Anton, A. Werner, and K. H. Schartner, *J. Phys. B* **27**, 4195 (1994).
- [15] J. Kuang and C. D. Lin, *J. Phys. B* **29**, 1207 (1996).
- [16] J. Kuang and C. D. Lin, *J. Phys. B* **29**, 5443 (1996).
- [17] I. B. Abdurakhmanov, A. S. Kadyrov, S. K. Avazbaev, and I. Bray, *J. Phys. B* **49**, 115203 (2016).
- [18] M. B. Shah and H. B. Gilbody, *J. Phys. B* **14**, 2361 (1981).
- [19] M. B. Shah, D. S. Elliott, and H. B. Gilbody, *J. Phys. B* **20**, 2481 (1987).
- [20] M. B. Shah, J. Geddes, B. M. McLaughlin, and H. B. Gilbody, *J. Phys. B* **31**, L757 (1998).
- [21] K. Omidvar, *Phys. Rev.* **153**, 121 (1967).